PNAS
www.pnas.org

Supplementary Information for

Structural Basis for IFN Antagonism by Human Respiratory Syncytial Virus Nonstructural Protein 2

Jingjing Pei[1], Nicole D. Wagner[2], Angela J. Zou[3], Srirupa Chatterjee[1], Dominika Borek[4], Aidan Cole[3], Preston J. Kim[3], Christopher F. Basler[5], Zbyszek Otwinowski[4], Michael L. Gross[2], Gaya K. Amarasinghe[3], and Daisy W. Leung[1,3]*

[1]John T. Milliken Department of Medicine, Division of Infectious Diseases, Washington University School of Medicine, St. Louis, MO 63110, USA

[2]Department of Chemistry, Washington University in St. Louis, St. Louis, MO 63110, USA

[3]Department of Pathology and Immunology, Washington University School of Medicine, St. Louis, MO 63110, USA

[4]Department of Biophysics, University of Texas Southwestern Medical Center, Dallas, TX USA 75390, USA

[5]Center for Microbial Pathogenesis, Institute for Biomedical Sciences, Georgia State University, Atlanta, GA 30303, USA.

*corresponding author
Email: dwleung@wustl.edu

This PDF file includes:

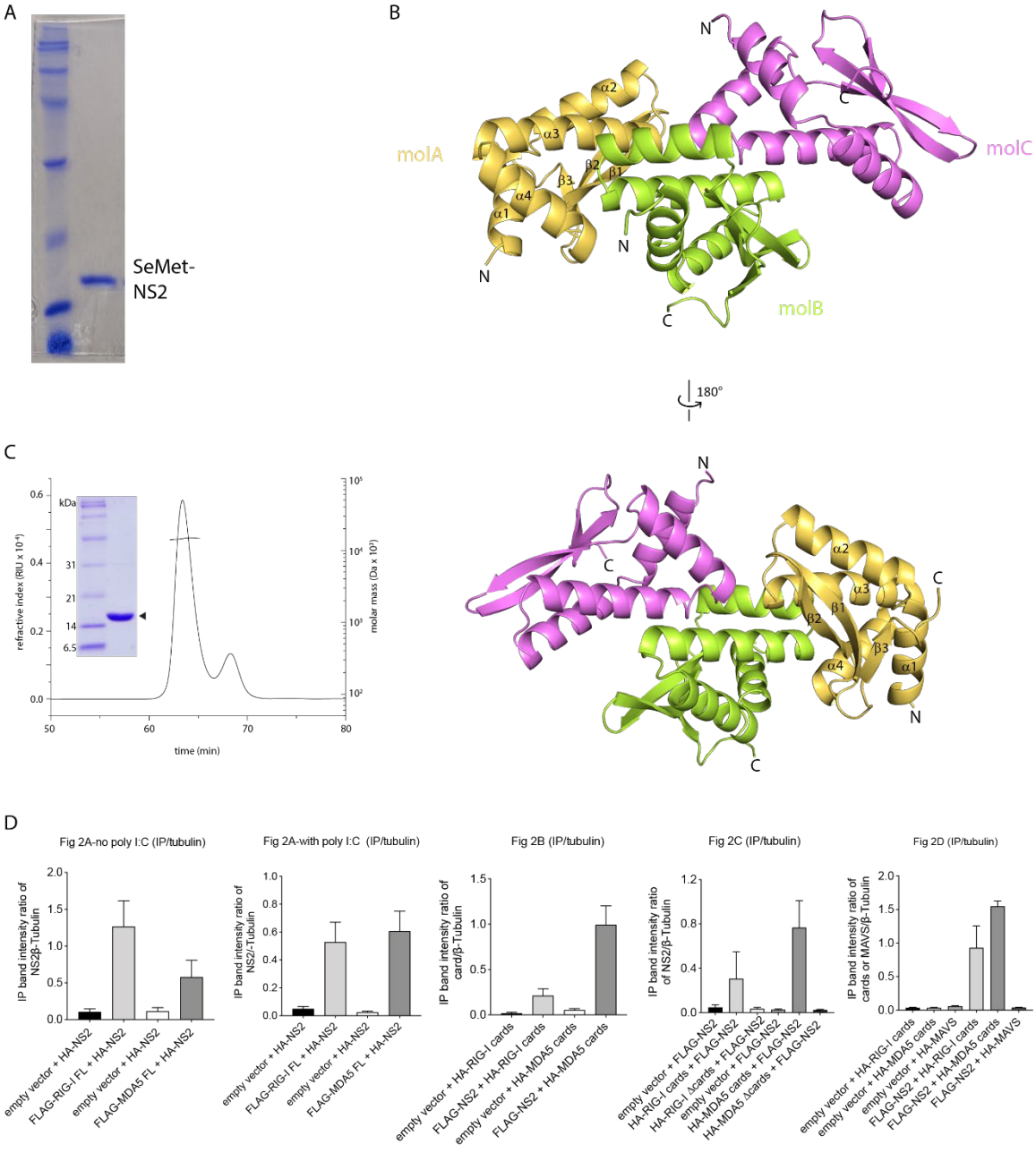

Figure S1. Analysis of RSV NS2 X-ray crystal structure. A. Coomassie-stained SDS-PAGE of purified selenomethionine-labeled NS2 protein. **B.** The crystallographic asymmetric unit contains three molecules of NS2. Molecule A, yellow; molecule B, green; molecule C, pink. **C.** Size exclusion chromatography coupled to multiangle light scattering analysis of recombinantly expressed and purified NS2 demonstrates an experimentally determined molecular weight of 14.6 kDa. The theoretical molecular weight of NS2 is 14.9 kDa. **D.** Image analysis of quantification of Western blot bands in Fig. 2 using ImageJ and GraphPad Prism 8.

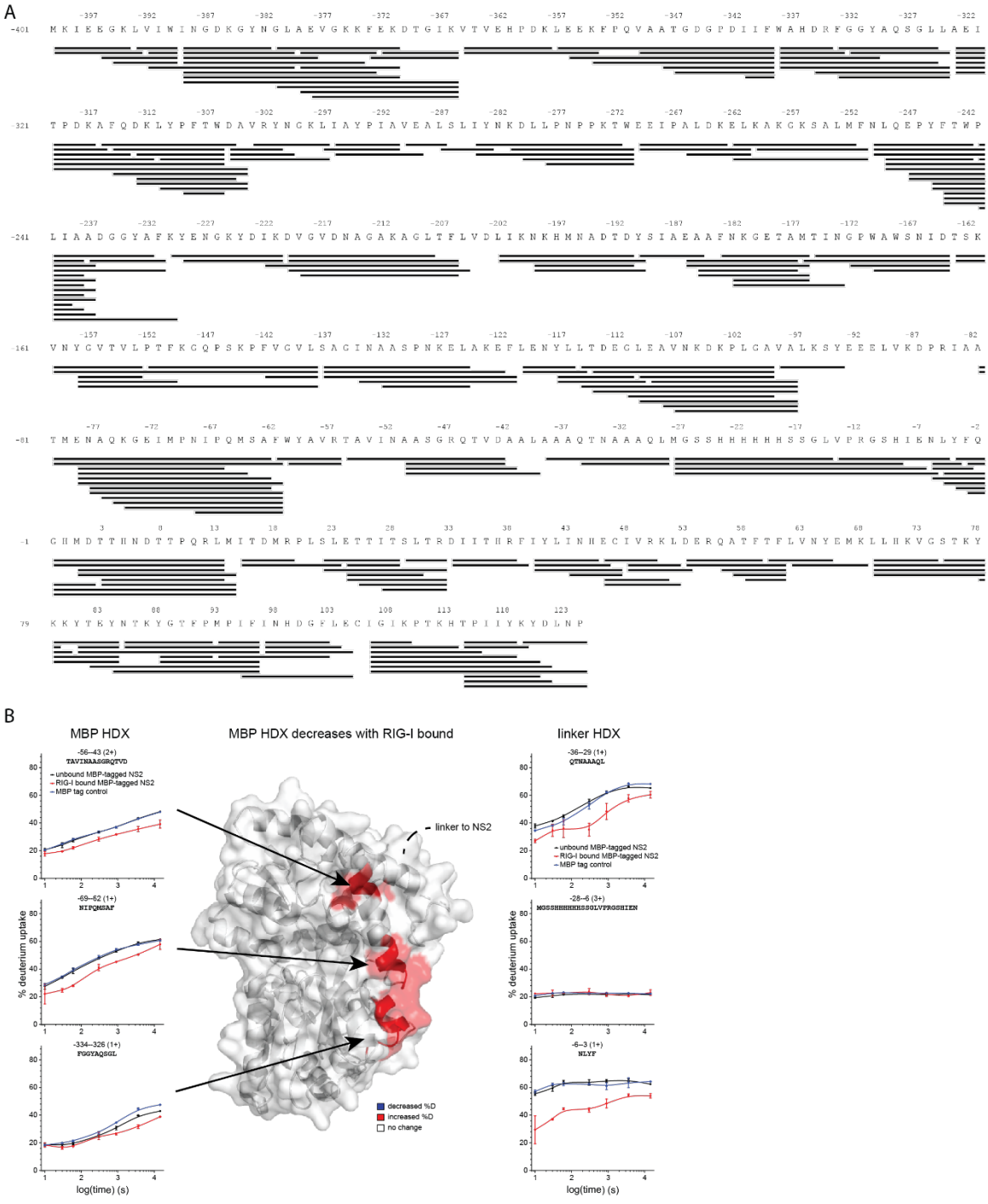

Figure S2. Peptide coverage analysis of NS2 by bottom-up analysis and impact of MBP fusion tag on NS2 HDX. A. Coverage map showing all LC-MS/MS identified digestion products with valid HDX results. **B.** HDX kinetics curves for the shortest MBP peptides that indicate any difference in deuterium uptake and consistent with other overlapping peptides (left column). Observed decreases in MBP peptide deuterium uptake for the MBP tag control vs. RIG-I CARDs bound MBP-tagged NS2 mapped onto an MBP structure (PDB 3PGF) (middle column). C. HDX kinetics curves for linker peptides (right column).

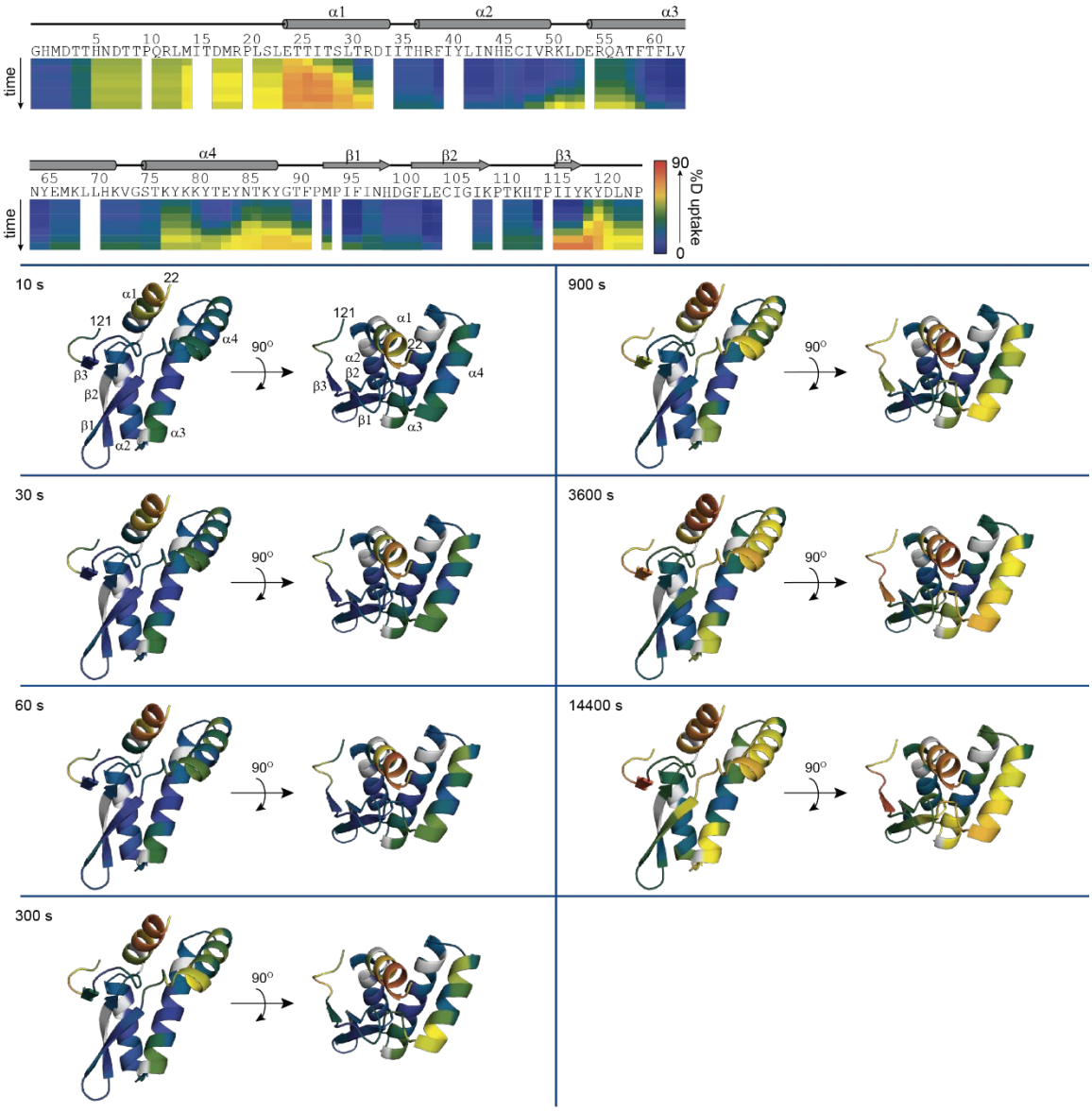

Figure S3. HDX-MS of RSV NS2 reveals regions that are dynamic and protected upon binding to RIG-I CARDs for all time points collected. Heatmap showing the extent of HDX for free NS2 for incubation times of 10, 30, 60, 300, 900, 3600, and 14400 s. The heat maps were smoothed using "light smoothing" with the HDExaminer software. Secondary structures determined in the crystal structure are shown above. Deuterium uptake extents mapped onto the NS2 structure are shown here for all times points collected.

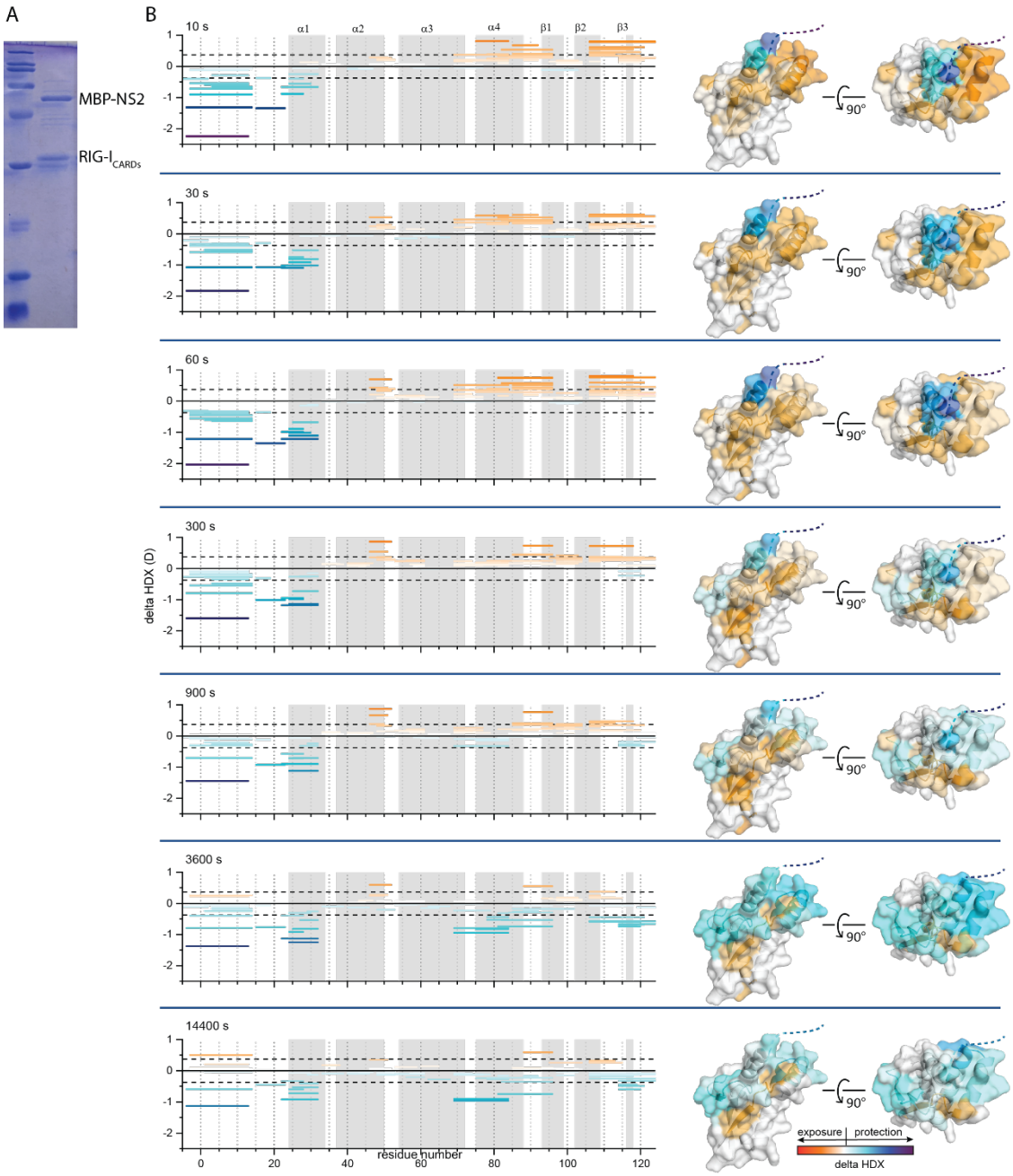

Figure S4. Peptide-level difference maps showing absolute differences in HDX for all identified peptides after all time points collected of HDX (top to bottom). A. Coomassie-stained SDS-PAGE of MBP-NS2/RIG-ICARDs complex. **B.** A peptide-level summary of all differential HDX results (in Da) for NS2 unbound vs. NS2 bound to RIG-I CARDs. Each peptide is shown as a bar covering the peptide sequence. Global significance limits (black dash) indicate the minimum HDX difference to be statistically significant ($p < 0.01$). Increases (warm) and decreases (cool) in HDX are indicated by the gradient and corresponds to the structures on the right. Secondary structural elments are shaded in gray. Representative peptide-level increases (warm colors) and decreases (cool colors) in HDX as a function of binding RIG-I CARDs mapped onto the crystal structure of NS2 after all times points collected of exchange. Structures on the right are shown in the same orientation as those in Fig. 5B and are rotated 90° along the y-axis on the right.

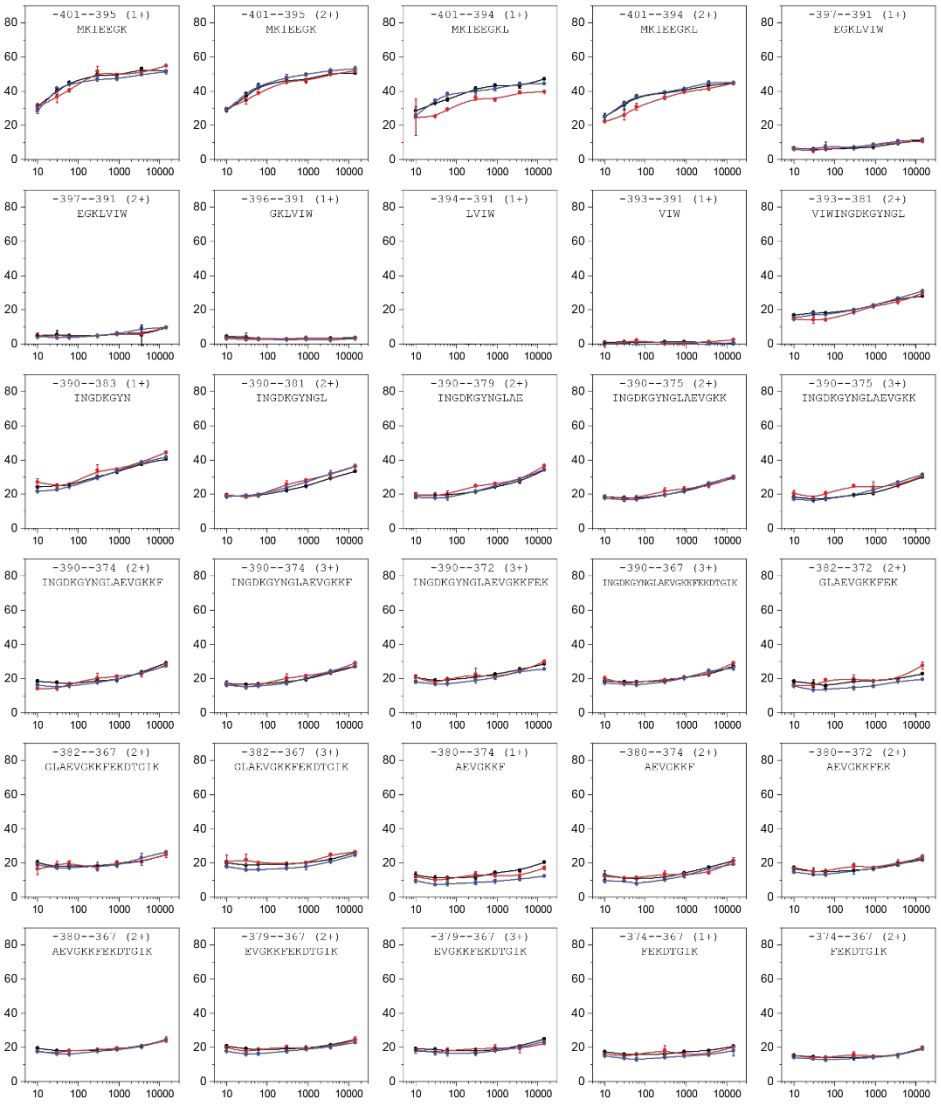

Figure S5.1 HDX kinetics curves of all peptides covering MBP-tagged NS2. Unbound, black; copurified with RIG-I CARDs (red); and MBP control (blue).

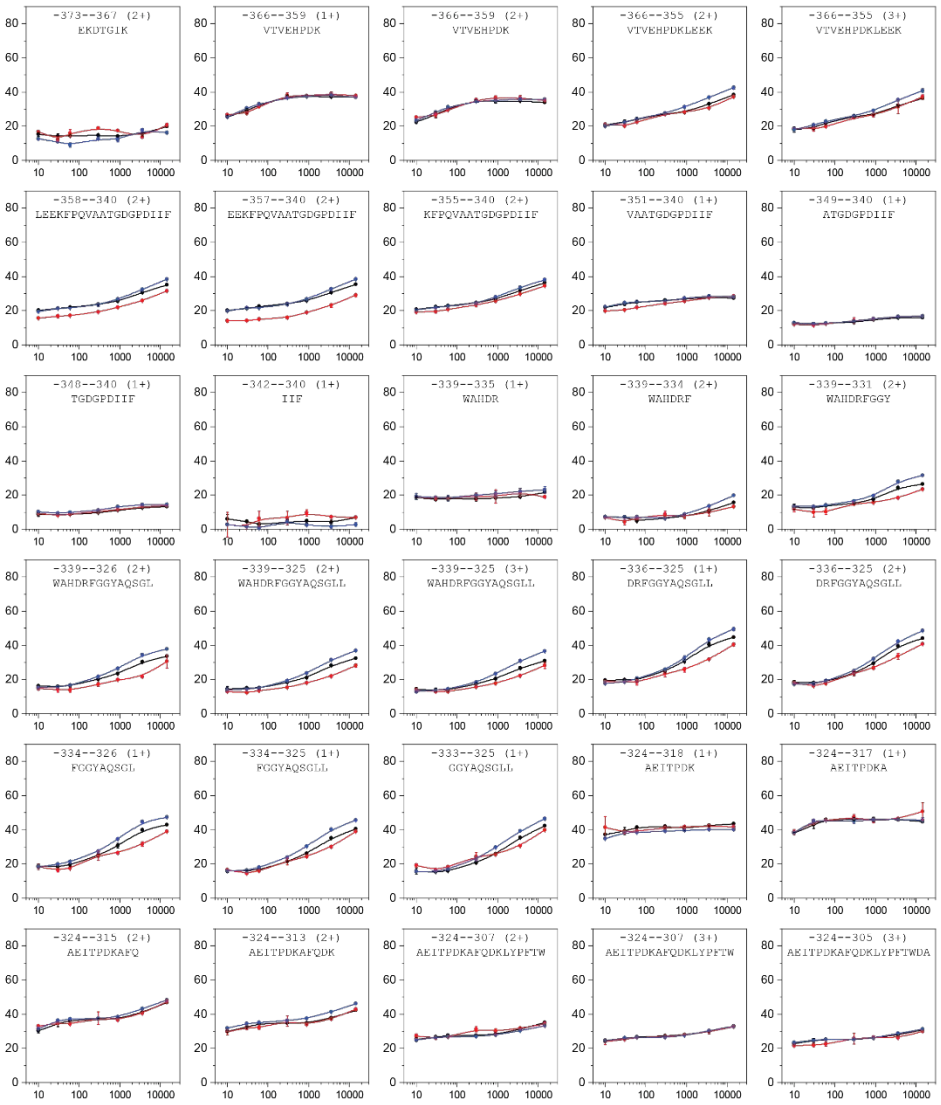

Figure S5.2 HDX kinetics curves of all peptides covering MBP-tagged NS2. Unbound, black; copurified with RIG-I CARDs (red); and MBP control (blue).

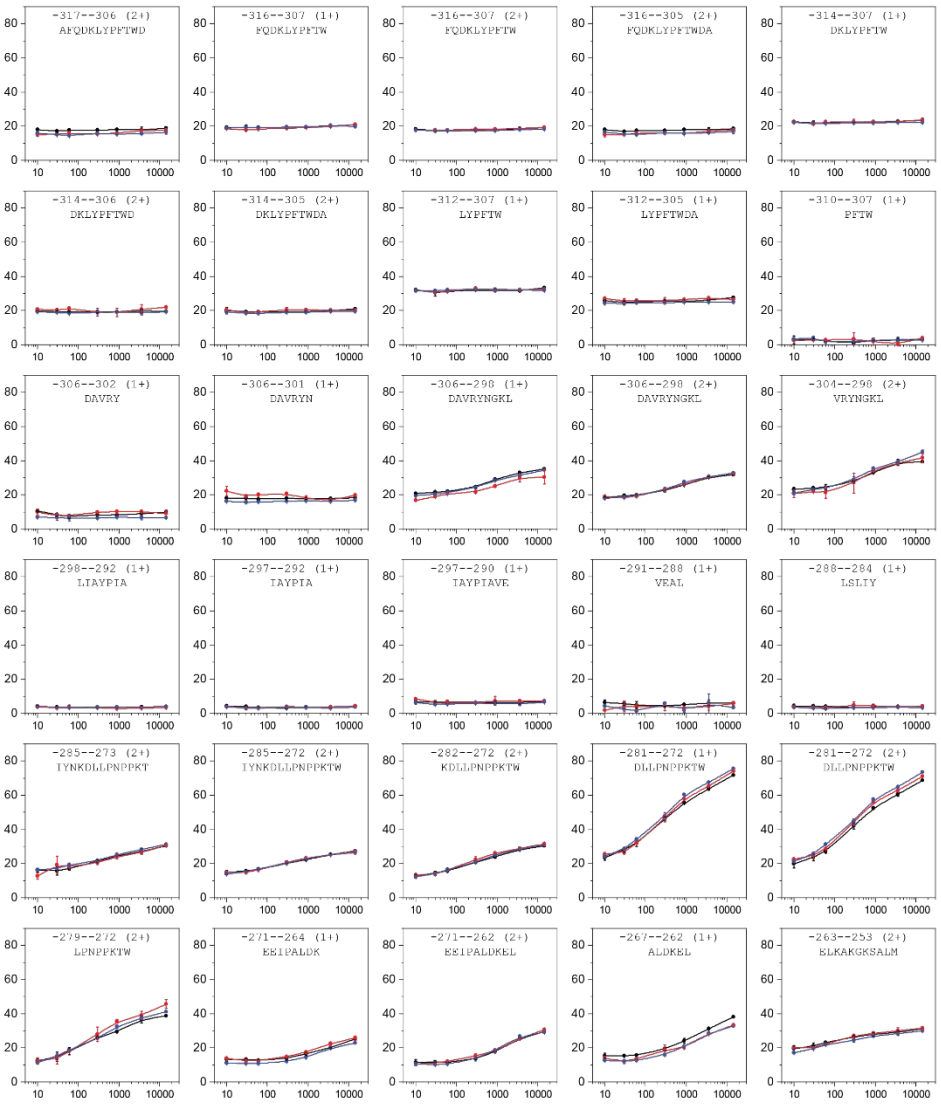

Figure S5.3 HDX kinetics curves of all peptides covering MBP-tagged NS2. Unbound, black; copurified with RIG-I CARDs (red); and MBP control (blue).

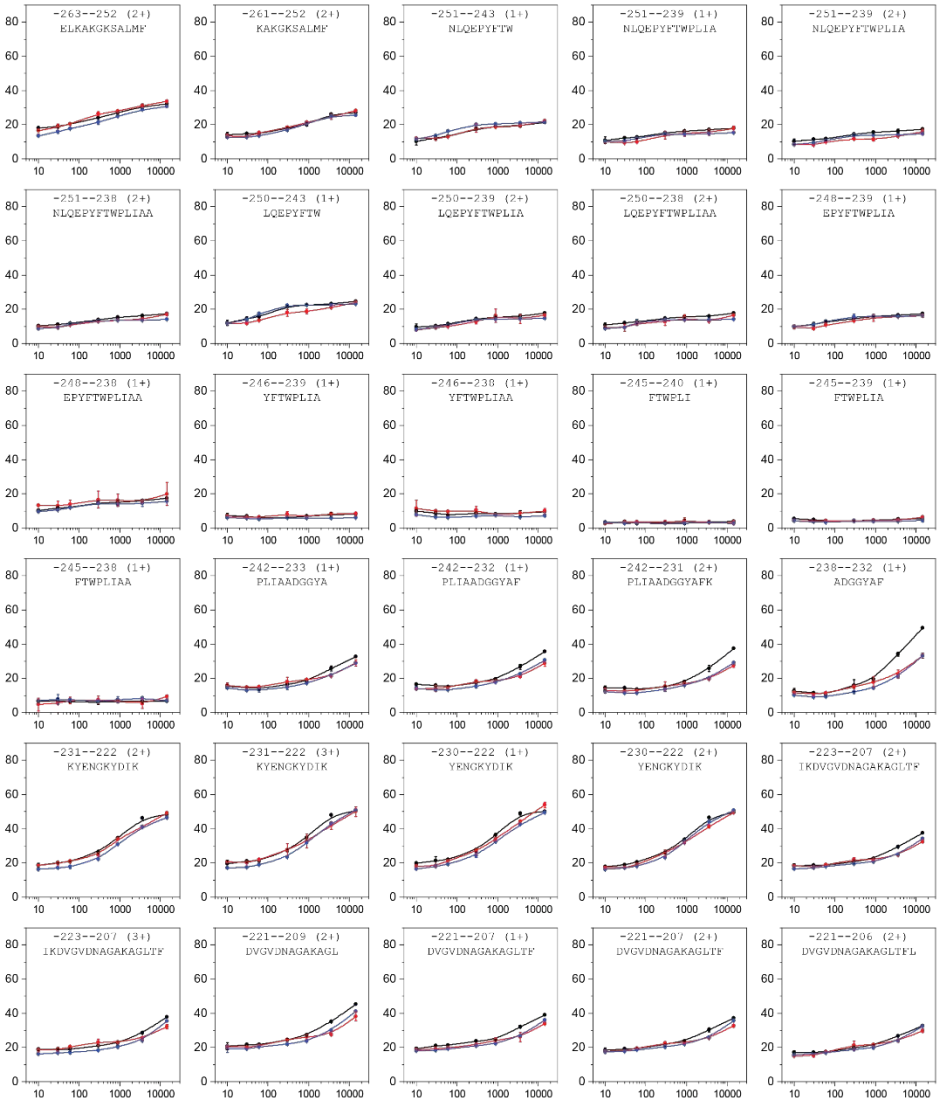

Figure S5.4 HDX kinetics curves of all peptides covering MBP-tagged NS2. Unbound, black; copurified with RIG-I CARDs (red); and MBP control (blue).

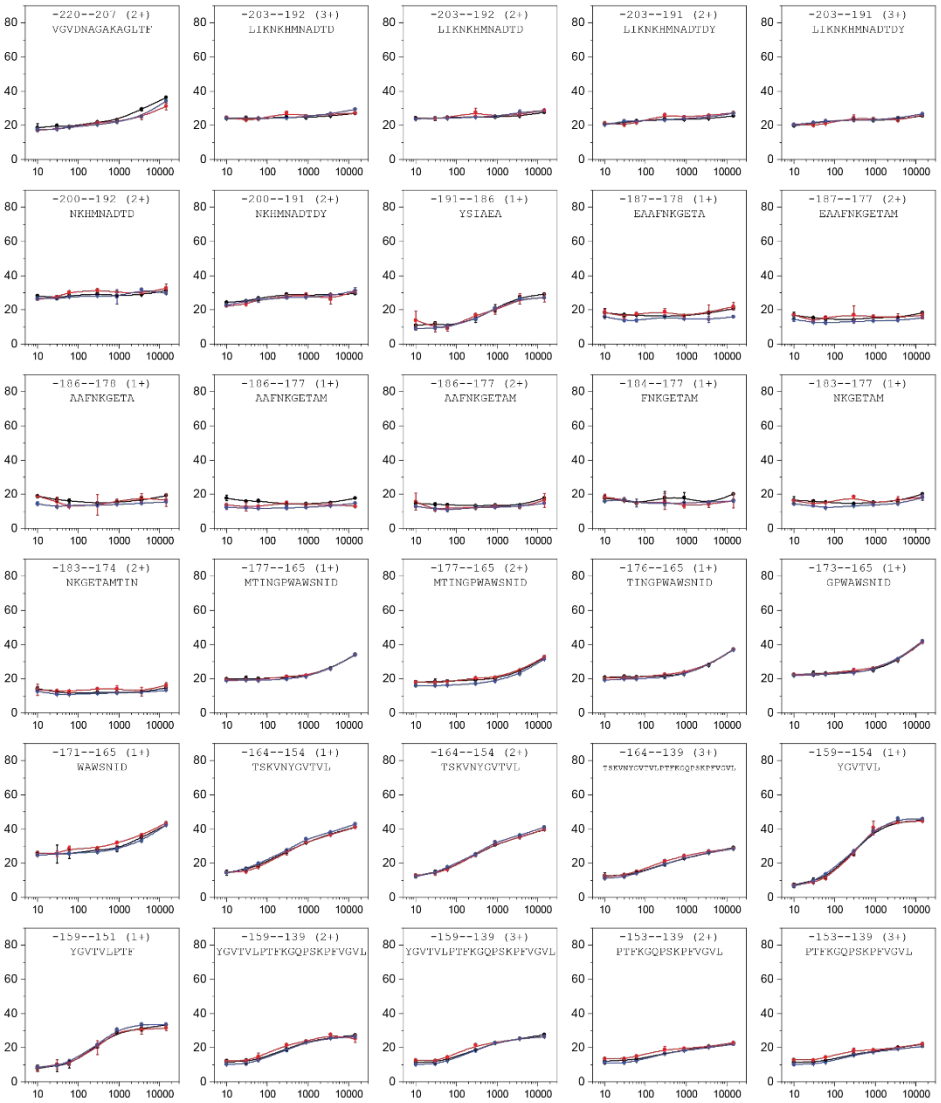

Figure S5.5 HDX kinetics curves of all peptides covering MBP-tagged NS2. Unbound, black; copurified with RIG-I CARDs (red); and MBP control (blue).

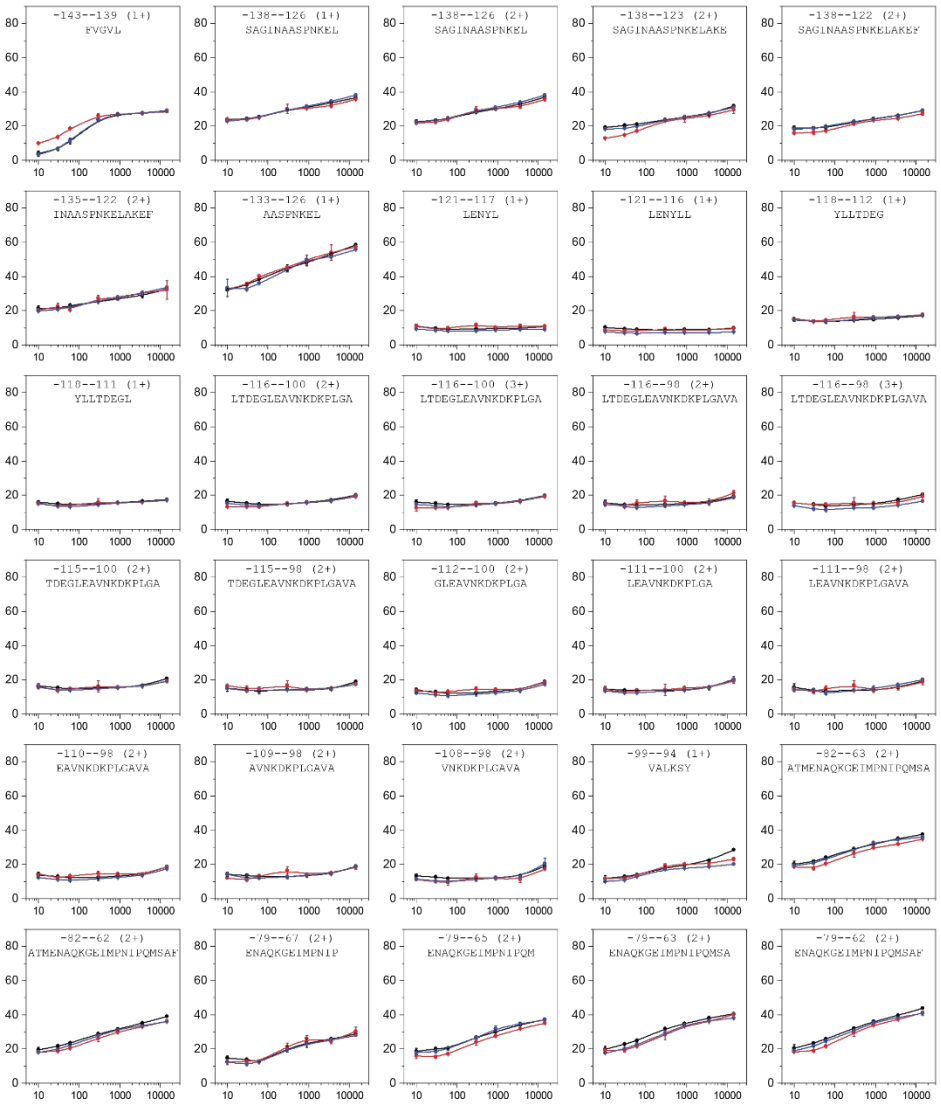

Figure S5.6 HDX kinetics curves of all peptides covering MBP-tagged NS2. Unbound, black; copurified with RIG-I CARDs (red); and MBP control (blue).

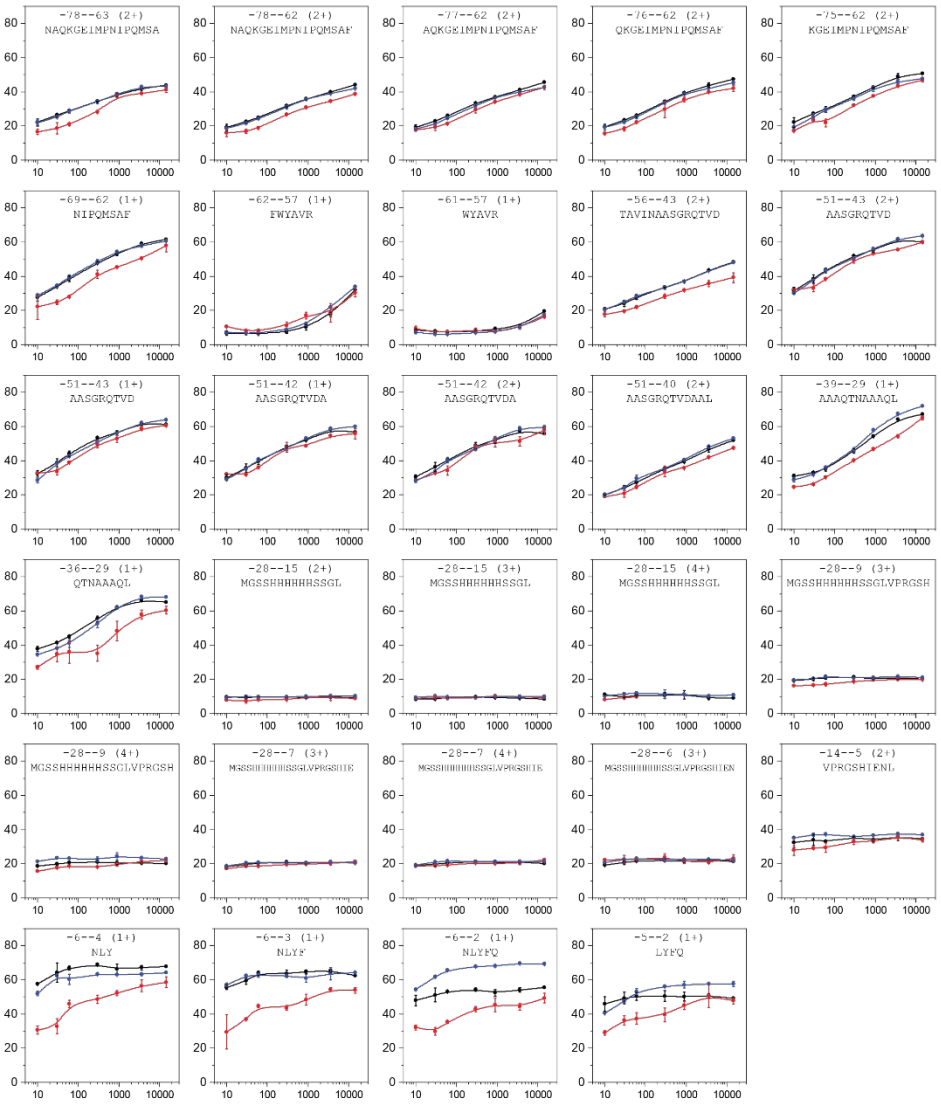

Figure S5.7 HDX kinetics curves of all peptides covering MBP-tagged NS2. Unbound, black; copurified with RIG-I CARDs (red); and MBP control (blue).

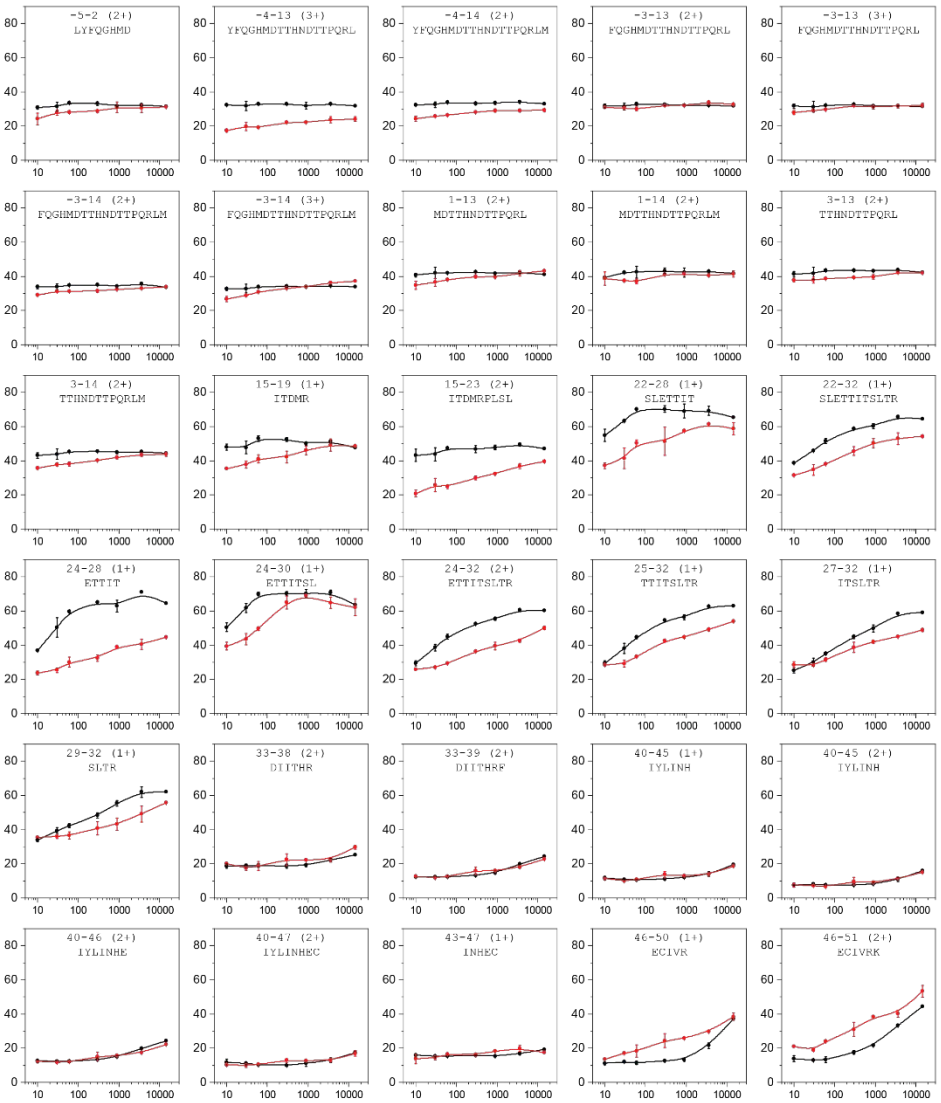

Figure S5.8 HDX kinetics curves of all peptides covering MBP-tagged NS2. Unbound, black; copurified with RIG-I CARDs (red).

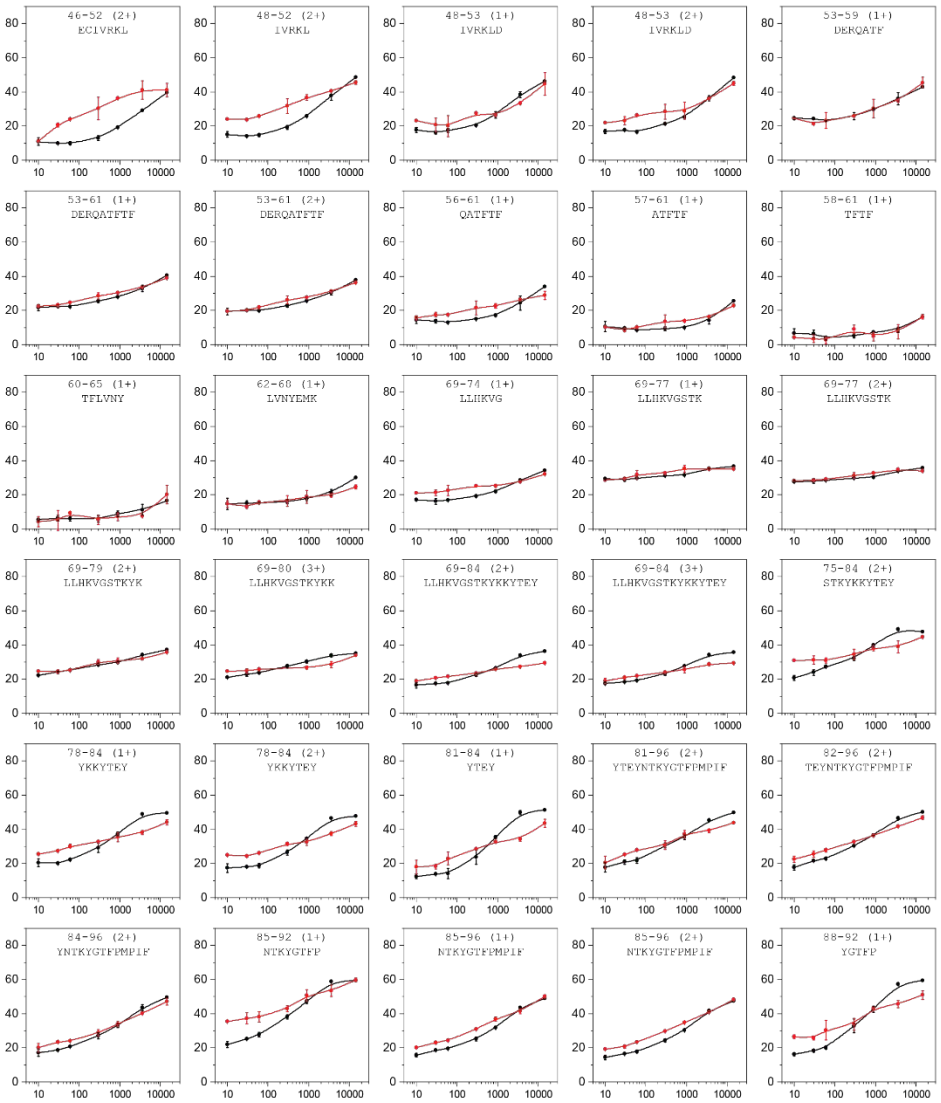

Figure S5.9 HDX kinetics curves of all peptides covering MBP-tagged NS2. Unbound, black; copurified with RIG-I CARDs (red).

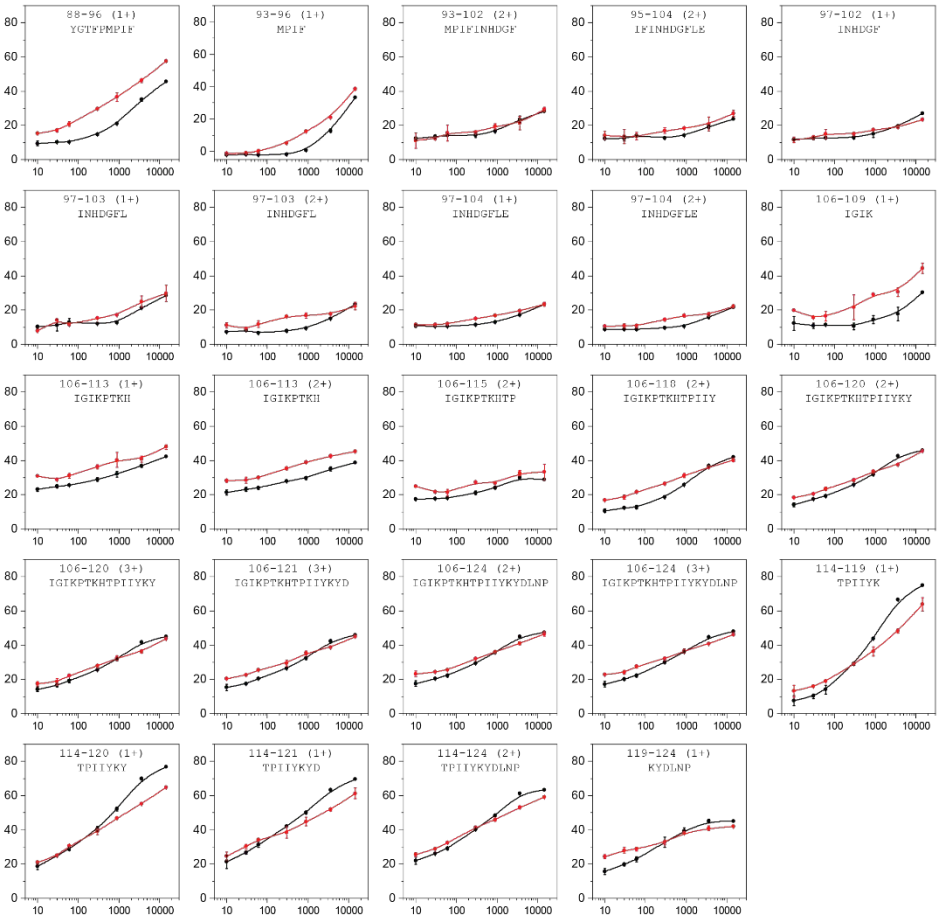

Figure S5.10 HDX kinetics curves of all peptides covering MBP-tagged NS2. Unbound, black; copurified with RIG-I CARDs (red).

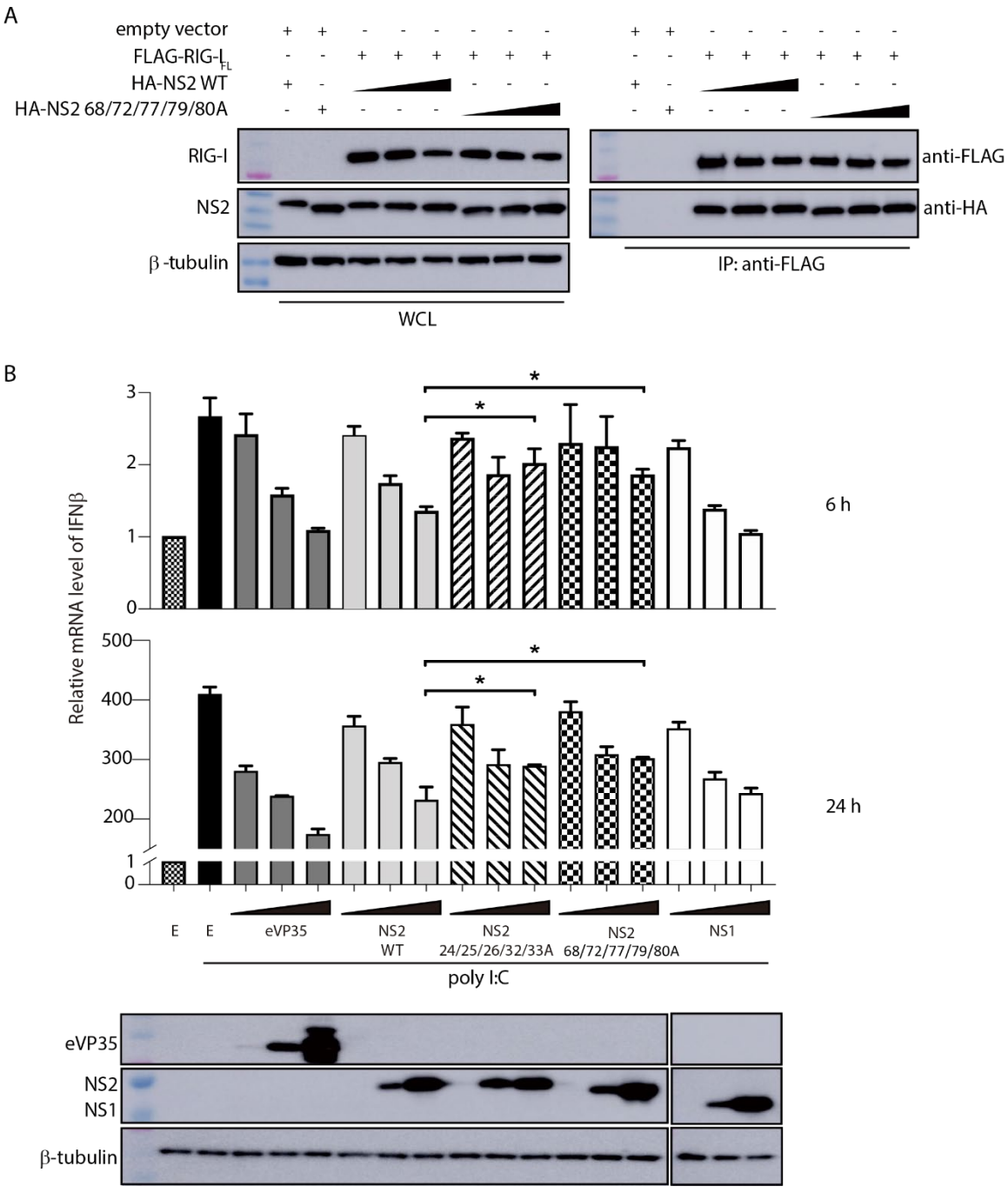

Figure S6. NS2 mutations outside of the N-terminus do not impact binding to RIG-I. A. Immunoblot of Flag-RIG-I coIPs in the presence of increasing concentrations of NS2 WT, NS2 68/72/77/79/80A (right). WCL (left), whole cell lysate. Shown are representative results from experiments repeated in triplicate. **B.** qRT-PCR of IFNβ mRNA levels of 293T cells transfected with increasing concentrations (0.2, 1, and 5 μg) of eVP35 (control IFN antagonist), NS2 WT, NS2 24/25/26/32/33A mutant, NS2 68/72/77/79/80A mutant, or NS1 and poly I:C treatment. The data represent the mean ± SEM of 3 independent experiments. Unpaired t-test; *$p < 0.05$. Western blots of protein expression are shown below.

Table S1. Data collection, structure solution, and refinement statistics.

Data collection	
Space Group	$P6_2$
Unit cell parameters	
a, b, c (Å)	157.65， 157.65，47.29
α, β, γ (°)	90, 90, 120
Resolution range (Å)[1,2]	50.00 – 2.80 (2.85 – 2.80) II c ~3.2; II a, b ~2.8
Unique reflections	16685 (740)
Redundancy	7.1 (5.9)
Completeness (%)	99.4 (91.1)
R_{merge} (%)	8.3 (N/A)[3]
$I / I\sigma$	24.8 (0.82)
Sharpening B-factors (Å^2)	-113.2 II c, -86.3 II a, b
Structure solution and refinement	
Resolution (Å)	45.55 – 2.82 (2.89 – 2.82)
No. of reflections	13610 (172)
Completeness (%)	86.11 (15.01)[4]
non-hydrogen atoms	2711
R_{work} / R_{free} (%)	21.2 / 25.6 (30.3 / 21.80)
R.m.s. deviations	
Bond lengths (Å)	0.01
Bond angles (°)	1.59
B-factors (Å^2)	
Protein Chain A	51.
Chain B	50.2
Chain C	68.5
Water	38.1
Ramachandran plot outliers (%)	0.00
Molprobity score	1.97
Molprobity clashscore	5.97

[1] Values in parentheses are for the highest resolution shell.
[2] The resolution is reported in two different directions because of the strong anisotropy.
[3] The high crystallographic symmetry and high redundancy result in the values of R_{merge} exceeding 1.000. And such values do not have statistical sense, therefore we report them as NA.
[4] Please note that the nominal completion is very high i.e. we collected and processed a complete data set. However, we used elliptical truncation before refinement and that kept only ~15% of reflections at high resolution.